Journal of Power Sources 390 (2018) 30–37

Contents lists available at ScienceDirect

Journal of Power Sources

journal homepage: www.elsevier.com/locate/jpowsour

Efficiency improvement of an all-vanadium redox flow battery by harvesting low-grade heat

Danick Reynard, C.R. Dennison, Alberto Battistel*, Hubert H. Girault

Ecole Polytechnique Federale de Lausanne (EPFL), Laboratoire d'Electrochimie Physique et Analytique (LEPA), Rue de l'Industrie 17, CH-1951, Sion, Switzerland

HIGHLIGHTS

- A *Thermally Regenerative Electrochemical Cycle* combined with a *V-Redox Flow Battery*.
- Operation between 20 and 60 °C.
- Comparison of a *Commercial* and a *Mixed-Acid Electrolyte*.
- Efficiency gain of 9% points (1.3 Wh L^{-1}) for the *Commercial Electrolyte*.
- Efficiency gain of 5% points (0.8 Wh L^{-1}) for the *Mixed-Acid Electrolyte*.

GRAPHICAL ABSTRACT

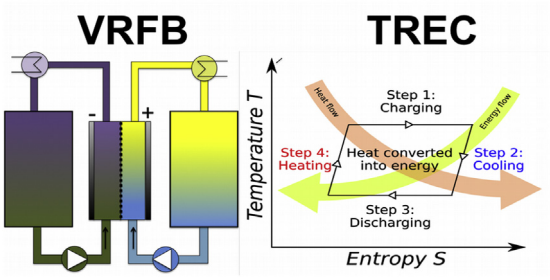

ARTICLE INFO

Keywords:
All-vanadium redox flow battery
VRFB
Thermally regenerative electrochemical cell
TREC
Mixed-acid electrolyte

ABSTRACT

Redox flow batteries (RFBs) are rugged systems, which can withstand several thousand cycles and last many years. However, they suffer from low energy density, low power density, and low efficiency. Integrating a Thermally Regenerative Electrochemical Cycle (TREC) into the RFB, it is possible to mitigate some of these drawbacks. The TREC takes advantage of the temperature dependence of the cell voltage to convert heat directly into electrical energy. Here, the performance increase of a TREC-RFB is investigated using two kinds of all-vanadium electrolyte chemistries: one containing a typical concentration of sulfuric acid and one containing a large excess of hydrochloric acid. The results show that the energy density of the system was increased by 1.3Wh L^{-1} and 0.8Wh L^{-1}, respectively and the overall energy efficiency also increased by 9 and 5 percentage points, respectively. The integration of the heat exchangers necessary to change the battery temperature is readily facilitated by the design of the redox flow battery, which already utilizes fluid circulation loops.

1. Introduction

Nowadays, traditional resources such as nuclear or fossil fuels are the most exploited energy resources for electricity generation, but their environmental impact exposes the world to serious concerns. Fortunately, the quest for renewable energy resources has become a priority to satisfy the continuous increase of energy demand [1,2]. However, the intermittent availability of renewable energy resources, such as wind or solar, seriously complicates their integration into large-scale electrical grids. Currently, the intermittence of energy demand is offset by allocating traditional generating capacity as 'operating reserves'. These reserves can respond quickly to a peak in energy demand. Nevertheless, they are both expensive and rather inefficient [2,3]. As an alternative, batteries are being strongly investigated to facilitate the integration of renewable energy sources, by storing energy during periods of high supply, and supplying energy during periods of shortage. To-date, lithium-ion batteries (Li-ion), sodium-sulfur batteries (Na-S), and redox flow batteries (RFB) have received the greatest consideration for large scale energy storage due to their favorable characteristics (Table 1) [2,4].

* Corresponding author.
E-mail addresses: alberto.battistel@epfl.ch, alberto.battistel@rub.de (A. Battistel).

https://doi.org/10.1016/j.jpowsour.2018.03.074
Received 17 January 2018; Received in revised form 7 March 2018; Accepted 27 March 2018

Table 1
Technical characteristics for Lithium-ion (Li-ion), Sodium-Sulfur (Na-S) and Redox Flow Battery (RFB) [4–6].

	E density [Wh kg^{-1}]	Cycle life-time	Operating *T* [°C]
Li-ion	100 to 200	600 to 1200	−10 to 40
Na-S	120 to 150	2500 to 4500	300 to 350
RFB	10 to 50	> 10000	10 to 50

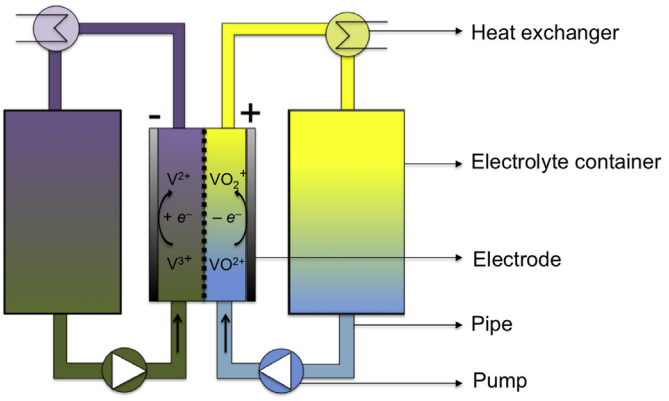

Fig. 1. Schematic of an all-vanadium redox flow battery (VRFB) during charging with two heat exchangers integrated in the piping system.

Redox flow batteries are distinct from Li-ion and Na-S batteries in that the former have a system architecture that includes tanks, pumps, a central reactor, *etc.*, which is analogous to many industrial chemical processes (Fig. 1). Long cycle lifetime is facilitated by the fact that the electrodes are inert spectators of the reaction, and the soluble redox species cannot be consumed. Despite these advantages, RFBs have difficulty competing with other batteries due to their low energy density.

Among the various RFB chemistries, the all-vanadium redox flow battery (VRFB) has received considerable attention (Fig. 1) [3,7]. First studied by Skyllas-Kazacos and co-workers in the 1970s, the VRFB is unaffected by cross-contamination of the redox species because it utilizes the same species on both the negative (V^{III}/V^{II}) and the positive side (V^{V}/V^{IV}) [1]. Commercial VRFB electrolyte typically contains *ca.* 1.6 M of the vanadium redox species in *ca.* 2 M sulfuric acid [8]. In acidic conditions, the following reactions take place at the electrode interface: [8]

$+$ *side* $\quad VO_2^+ + e^- + 2H^+ \rightarrow VO^{2+} + H_2O \quad E^0 = 1.00\,V$

$-$ *side* $\quad V^{3+} + e^- \rightarrow V^{2+} \quad E^0 = -0.26\,V$

Kausar et al. observed that adding *ca.* 1% phosphoric acid in the electrolyte solution increases the thermal stability of V^V [9]. Similarly, Pacific Northwest National Laboratory (PNNL) added a large excess of hydrochloric acid to the electrolyte yielding better vanadium solubility (2.5M) and a wider thermal range (−10 °C – +50 °C). In the presence of chloride, the resulting reactions taking place in the battery become: [10,11]

$+$ *side* $\quad VO_2Cl + e^- + 2H^+ \rightarrow VO^{2+} + Cl^- + H_2O$

$-$ *side* $\quad VCl_3 + e^- \rightarrow VCl_2 + Cl^-$

Although the standard potential for the vanadium redox couples in the mixed-acid electrolyte was not specified, it was noticed that the reversibility was comparable to the conventional electrolyte, and a small shift in potential for both redox couples was observed providing a larger cell voltage.

Apart from optimising the chemistry of the battery, one possibility to improve the performance is to focus on the thermodynamics of the battery. Taking advantage of the thermogalvanic effect, which is the temperature dependence of the cell voltage, it is possible to convert heat directly into electrical energy [12–14].

Usually a battery is charged and discharged at a constant temperature. However, the thermodynamic potential of the electrode reactions is dependent on the operating temperature. Based on this principle, a thermodynamic cycle may be designed by charging the battery at a higher or lower temperature than the discharge. In this cycle, traditionally-employed compression and expansion of a gas, *e.g.* Carnot cycle, is replaced by injection and harvesting of electrical charge (Fig. 2 a). Such a system is called Thermally Regenerative Electrochemical Cycle (TREC) and has been reviewed by Chum and Osteryoung in 1981 [15]. Yet, it was primarily studied for high-temperature heat recovery applications. However, to avoid potential overheating and evaporation, for an aqueous-base battery, low temperature heat is desirable. This is ubiquitously available as waste heat (low-grade heat < 100 °C) [14] from many industrial processes, although it requires large heat exchangers to be employed.

In recent years, several TRECs utilizing low-grade heat recovery were developed. In 2014, a TREC using copper hexacyanoferrate and Cu/Cu^{2+} electrodes for low-grade recovery application was proposed [13]. A similar cycle could be performed without membrane [16] or even without an external voltage input [17]. A TREC with supercapacitor was also demonstrated [18]. Long and Li performed several analyses on TREC systems [19].

A TREC can be readily applied to RFBs. As shown in Fig. 1, heat

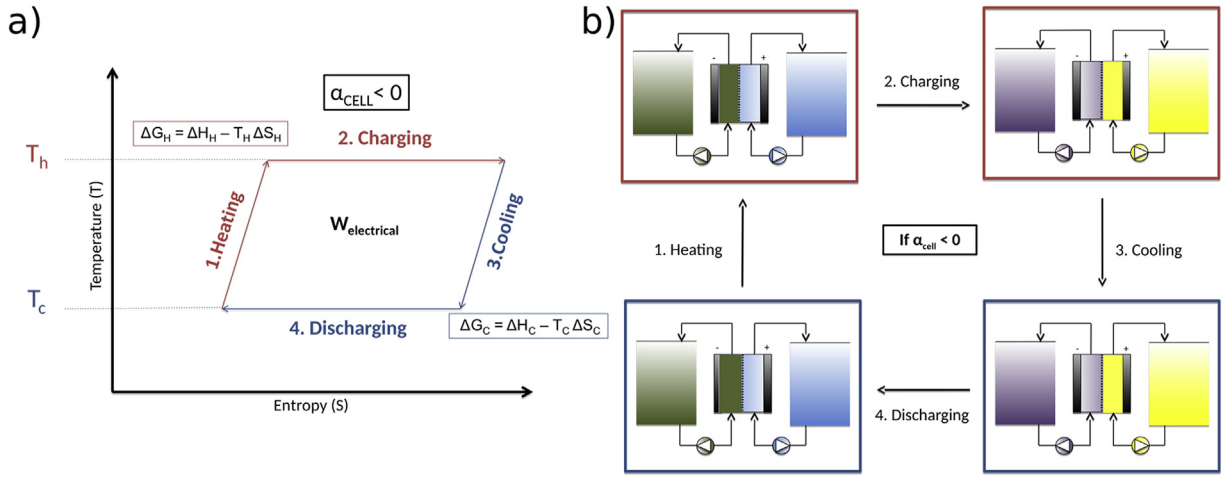

Fig. 2. Schematic of the thermodynamic cycle performed by a TREC (a) Temperature-entropy plot during a cycle performed by a TREC for $\alpha_{cell} < 0$ and $E_{cell} < E_{\Delta H}$ [13] (b) Schematic representation of the thermodynamic cycle performed by the TREC-VRFB.

exchangers can easily be implemented in a RFB. These heat exchangers would simply represent an extension of the existing piping system, with the electrolyte of the battery acting as one of the heat exchange fluids. A flow battery with ammonia as a heat scavenger was also used to build a TREC [20].

In this work, a TREC was applied to a vanadium redox flow battery (see Fig. 1). Two different electrolytes were compared: one containing 2 M H_2SO_4 and 50 mM H_3PO_4 and a second one also containing 4 M HCl. We refer to the first as *Commercial Electrolyte* (CE) as it is based on the most commonly-available electrolyte, and to the second one as *Mixed-Acid Electrolyte* (MAE), as it is similar to the formulation suggested by PNNL.

2. Theory

The temperature dependence of the electrode potential, E, is characterized by the thermal coefficient, α, defined as:

$$\alpha = \frac{\partial E}{\partial T} \tag{1}$$

Considering a half-cell reaction at an electrode interface, $A^{x+n} + ne^- \rightarrow B^x$, the resulting Gibbs free energy change is given by:

$$\Delta G = -nFE \tag{2}$$

which can also be represented as:

$$\Delta G = \Delta H - T\Delta S \tag{3}$$

where n is the number of electrons transferred, F is the Faraday's constant, E is the electrode potential, ΔH is the enthalpy change, $T\Delta S$ is the heat exchanged with the environment, T is the temperature, and ΔS corresponds to the entropy change for the half-cell reaction in isothermal conditions. As it was already noted, the entropic part of the Gibbs free energy is a key factor in electrochemical devices [21–24] and according to Eqs. (1)–(3), the thermal coefficient of the electrode, α, can be derived as follows:

$$\alpha = \frac{\partial E}{\partial T} = \frac{\Delta S}{nF} \tag{4}$$

For the whole cell reaction, the thermal coefficient is the combination of the two half-cell reaction thermal coefficients:

$$\alpha_{cell} = \alpha_+ - \alpha_- \tag{5}$$

Then, the thermoneutral potential, that represents the voltage at which the device neither absorbs nor reject heat, can be calculated as:

$$E_{\Delta H} = -\frac{\Delta H}{nF} = E - T\alpha_{cell} \tag{6}$$

The ability of the system to absorb or reject heat will directly depend on the relationship between the voltage applied at the leads of the battery, its thermoneutral potential, and the direction of the reaction (current). For a negative thermal coefficient, the different cases are described in Table 2.

Fig. 2 illustrates a 4-step TREC in which the full cell thermal coefficient is negative and the cell potential remains below the thermoneutral potential. Fig. 2a shows the thermodynamics and 2b the experimental realisation. In the first step, the system is in a discharged state and is heated (heat flux $Q > 0$) to an elevated temperature (T_H). For a VRFB, the tanks of the battery contain almost pure V^{III} on the negative side, which is dark green, and almost pure V^{IV} on the positive side, which is blue. Subsequently the battery is charged (step 2) by applying a positive current. Now, the negative side contains V^{II} (violet) and the positive side V^{V} (yellow). The third step represents the cooling of the system ($Q < 0$) to a cold temperature (T_C) and in the last step the cycle is closed with the discharge of the battery (negative current). The Gibbs free energy change during the charge and the discharge cycle are respectively given by ΔG_H and ΔG_C . The theoretical TREC performance of this cycle is characterized by the heat-to-electrical-work conversion efficiency (η_{TREC}), which corresponds to the extra net work recovered from the thermodynamic cycle over the thermal energy input [13].

Table 2
Specific relation between cell voltage (E) and thermoneutral voltage ($E_{\Delta H}$) during the charge and the discharge cycle of a battery [22].

	$E > E_{\Delta H}$	$E < E_{\Delta H}$
$i > 0$ (Charge)	Reject heat	Absorb heat
$i < 0$ (Discharge)	Absorb heat	Reject heat

$$\eta_{TREC} = \frac{W_{gained}}{Q_{rxn} + Q_{mass}} \tag{7}$$

The thermal energy required to perform the cycle includes the heat absorbed or rejected during the reaction by the system at T_H (Q_{rxn}) and the heat required to heat up the system (Q_{mass}). Neglecting the energy losses (electrical losses) of the battery cycle, the efficiency of the TREC can be written as follows:

$$\eta_{TREC} = \frac{\Delta T\Delta S}{T_H\Delta S + C_p\Delta T} \tag{8}$$

Where ΔS is the variation in entropy of the system, $\Delta T\Delta S$ is the maximum recovered electrical work, and C_p is the heat capacity at constant pressure of the battery (J K^{-1}). The losses of the battery also influence the heat-to-electrical-work conversion efficiency because some of the thermal energy, which is converted into electrical energy is later dissipated by the losses of the battery. As comparison, the Carnot efficiency (η_{Carnot}) is given by:

$$\eta_{Carnot} = \frac{\Delta T}{T_H} \tag{9}$$

Considering the specific charge capacity of the battery, q_c (C g^{-1}), the full thermal coefficient of the cell, α_{cell} (V K^{-1}), and the specific heat capacity of the battery system, C'_p (J K^{-1} g^{-1}), and that $\Delta S = \alpha_{cell}\cdot q_c$, the TREC efficiency can be written as:

$$\eta_{TREC} = \frac{\Delta T}{T_H + \frac{C'_p\Delta T}{\alpha_{cell}q_c}} \tag{10}$$

From Eq. (10), it is clear that a large thermal coefficient and large charge density coupled with a low heat capacity contribute to a high TREC efficiency. Unlike Lee et al., this formulation does not consider the existing inefficiency of the battery cycle, that is its energy losses. In fact, for systems with modest energy efficiencies, like redox flow batteries, the energy losses during cycling can be larger than the energy converted by the thermodynamic cycle, and the formulation suggested by Lee et al. would give a negative efficiency. Instead, the energy gained from the thermodynamic cycle should be considered relative to the isothermal cycle at the nominal operating temperature to give a normalised efficiency:

$$\eta'_{TREC} = \frac{(U_{D,TREC} - U_{C,TREC}) - (U_{D,20°C} - U_{C,20°C})}{T_H\alpha_{cell}q_c + C'_p\Delta T} = \frac{U_{NR}}{T_H\alpha_{cell}q_c + C'_p\Delta T} \tag{11}$$

where $U_{D,TREC}$ and $U_{C,TREC}$ are respectively the energy densities involved during discharging and charging steps of the TREC-VRFB cycle and $U_{D,20°C}$ and $U_{C,20°C}$ are the energy densities during operation of the VRFB at 20 °C. The sum of these terms is named the normalized energy recovered, U_{NR} (J g^{-1}), which implicitly depends on the efficiency of the VRFB at different temperatures. The normalized efficiency in Eq. (11) cannot be negative and represents the energy increase normalized by the total thermal input. To summarize, Eq. (9) gives the efficiency of converting heat into work and it represents the limit given by thermodynamics. Eq. (10) instead, considers the idealized efficiency that a TREC can achieve. As noted by Lee et al., the rightmost term in the denominator can be reduced by improving the heat transfer, for

example, or finding a chemical system with larger thermal coefficients. At last, the normalized efficiency of Eq. (11) signifies the actual figure of merit for a real system and represents how much this system can be improved compared with its normal operation at room temperature still taking into account the required thermal input.

3. Experimental method

Electrolyte Preparation: All of the solutions used were prepared from a commercial electrolyte (obtained from Gildemeister GmbH, Austria) composed of an aqueous solution of 1.6 M V^{IV}/V^{III} (*ca.* 50:50), 2 M sulfuric acid (H_2SO_4) and 50 mM phosphoric acid (H_3PO_4). Some undisclosed compounds and impurities were present in low amount. V^V and V^{II} solutions were electrochemically prepared first by galvanostatic and subsequent potentiostatic electrolysis of the commercial electrolyte in a flow cell with carbon felt electrodes (active area: 15 cm^2) and Nafion 115 membrane at a current density of 40 $mAcm^{-2}$, and with a cell voltage limitation of 1.6 V. These were used for the preparation of all the other solutions. Two different electrolytes were prepared by dilution: the so-called *Commercial Electrolyte* (CE) (1 M total vanadium, 2 M H_2SO_4, 50 mM H_3PO_4) and *Mixed-Acid Electrolyte* (MAE) (1 M total vanadium, 4 M HCl, 2 M H_2SO_4, 50 mM H_3PO_4).

Thermal coefficient study: The thermal coefficients of each redox couple were measured for both CE and MAE by studying the evolution of the equilibrium potential between 25 °C and 55 °C under nitrogen atmosphere. The equilibrium potential was measured through linear galvanodynamic scans at 0.01 mA s^{-1} between −0.1 mA s^{-1} and 0.1 mA s^{-1} in a 3-electrode setup with a glassy carbon working electrode, a carbon felt counter electrode, and a Ag|AgCl reference electrode. Then, a linear regression of the resulting measurements was performed to get an accurate value of the potential of zero current which, in the case of highly concentrated vanadium solution (0.5 M), was considered to be a good approximation of the equilibrium potential of the redox couple of interest. The working electrode was polished before each experiment with 3 μ m and 1 μ m abrasive paper (UltraPrep™ Diamond Lapping Films).

TREC-VRFB study: All the experiments were performed in a flow cell with graphite current collectors and carbon felt electrodes (15 cm^2) on both sides. The carbon felt electrodes were treated at 400 °C in air for 45 h. The membrane was Nafion 115 and was first pretreated in 3% H_2O_2 for 30 min at 80 °C and then in 0.5 M H_2SO_4 for 1 h at 95 °C. Silicone gaskets were used to seal the cell and to avoid leakage of electrolyte. Polycarbonate plates were used to hold all the cell components together (see ESI for details). Nitrogen gas was bubbled within the negative electrolyte tank. The reference electrode was placed in the positive tank and the negative side was wired as working electrode. The electrolyte was pumped through the cell using a peristaltic pumped (Ismatec-MCP). Before entering the cell, the electrolyte was circulated through heat exchangers in order to be heated or cooled. The heat exchangers were made of borosilicate glass and the heating or the cooling step was tested to last about 0.05 min mL^{-1} of electrolyte at a flow rate of 80 mL min^{-1}. To evaluate the battery performance at different temperatures, the all-vanadium redox flow battery was cycled at a constant current of 40 mA cm^{-2} several times at each temperature (20 °C and 60 °C) between 10 and 85% state of charge (SOC). Each experiment started with 1 M V^V electrolyte (about 80 mL) on the positive side and 1 M V^{II} electrolyte on the negative side. To ensure that the cell capacity was always limited by the positive half-cell, the amount of negative electrolyte was slightly larger than the positive electrolyte volume (about 10%). For the TREC cycles, the system was first heated to 60 °C (T_H) and then charged at constant current to reach the charge voltage (V_{Charge}). After charging, the system was cooled to 20 °C (T_C) and discharged galvanostatically to reach $V_{Discharge}$. To avoid any crossover effect, the electrochemical cell was drained during heating and cooling.

Electrochemical and temperature-control setup: All the electrochemical experiments were performed with a Biologic SP-300 potentiostat. The setup was heated up and cooled down with a recirculating chiller (MultiTemp III- Pharmacia Biotech) and the temperature was monitored with a temperature probe (IKA ETS-D5). As reference electrode a Ag|AgCl 3 M KCl with a double junction was employed. The junction was composed of a long borosilicate capillary filled with the same electrolyte as the solution of study, but without vanadium species. The capillary was long enough to avoid any temperature variation in the Ag|AgCl.

4. Results and discussion

Thermal stability study: For the *commercial electrolyte*, it has been reported that V^V is not stable at elevated temperatures and tends to convert to vanadium pentoxide (V_2O_5) [8,25,26]. It was noticed that V^V precipitates as vanadium pentoxide from a solution of 1.6 M after 4 h at 60 °C, whilst it was more stable at 1 M (8 h). Lowering the oxidation state of the solution also helped. Indeed, a solution made of 1 M V^V/V^{IV} (90:10) (90% SOC) did not show any noticeable precipitation after 4 h at 60 °C (see ESI for details). In the case of the *mixed-acid electrolyte*, V^V was much more stable in solution and no precipitation was noticed after 20 h at 60 °C with 1 M V^V. However, at this temperature, chlorine was evolved according to:

$$2VO_2Cl + 4H^+ \rightarrow 2VO^{2+} + Cl_2 + 2H_2O$$

lowering the oxidation state of the solution. However, the ratio V^V/V^{IV} (90:10) (90% SOC) was found to be stable for 22 h at 60 °C, and no further evolution of chlorine was observed. This was taken as upper limit of the composition of the positive electrolyte. According to this study, the state of charge for the battery was limited to 85%, the maximum temperature to 60 °C, and the length of the cycle to *ca.* 4 h.

Thermal coefficient study: The thermal coefficient of the vanadium redox couple was estimated based on the variation of the equilibrium potential with temperature. As shown in Fig. 3, the resulting thermal coefficient was determined to be −0.15(1) mV K^{-1} for the positive side and 1.01(7) mV K^{-1} for the negative side in the case of CE. The corresponding full-cell thermal coefficient was measured to be −1.16(8) mV K^{-1}. In a similar way, the thermal coefficients for the MAE were measured to be 0.025(10) mV K^{-1} on the positive side and 0.82(6) mV K^{-1} on the negative side. Thus, the resulting full cell thermal coefficient for the *mixed-acid electrolyte* was measured to be −0.80(7) mV K^{-1}. For both MAE and CE, the cell thermal coefficient was dominated by the negative electrolyte, which may be due to the solvation of the highly charged species. In the case of MAE, the positive electrolyte thermal coefficient was positive and therefore reduced the whole cell thermal coefficient, but its value was very close to zero. All of the thermal coefficients found in this study differed significantly from those reported in literature, which were −0.901 mV K^{-1} for V^V/V^{IV} and 1.5 mV K^{-1} for V^{III}/V^{II} [27]. It is worth noting, however, that these literature values were tabulated for unity activity and temperature variation of the standard potential, whereas the coefficients reported here are measured in high ionic strength electrolytes. Also the value reported from Bratsch for V^{III}/V^{II} was calculated, as opposed to experimentally measured.

Moreover, the thermal coefficients varied with the choice of the electrolyte confirming the fact that the chemical complexes formed in solution with chlorides are different [11].

Furthermore, with MAE, the whole-cell equilibrium potential was significantly different that with CE. The potential of the negative side was −0.45 V at room temperature and that of the positive one 0.99 V giving an overall increase of about 60 mV. From these results, a thermoneutral potential of 1.72 V for CE and of 1.67 V for MAE was estimated. All the results are summarized in Table 3. To avoid side reactions like hydrogen and oxygen evolution and degradation of the electrode material, in usual operation a VRFB works below 1.65 V. Therefore, a VRFB always operates according to the rightmost column

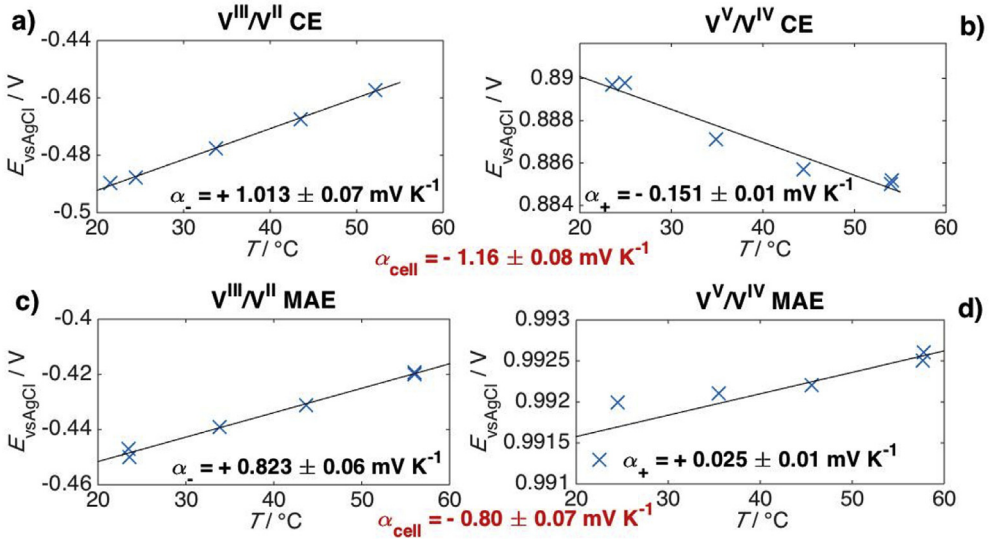

Fig. 3. Formal potential evolution with temperature (a) *commercial electrolyte* (CE) positive side (b) *commercial electrolyte* (CE) negative side (c) *mixed-acid electrolyte* (MAE) positive side (d) *mixed-acid electrolyte* (MAE) negative side.

Table 3
Composition and thermodynamic properties for *commercial electrolyte* and *mixed-acid electrolyte*.

	Heat capacity [J $mL^{-1}K^{-1}$]	Thermal coefficient [mV K^{-1}]	Equilibrium voltage @ 20 °C [V]	Thermoneutral voltage [V]
CE	4.2	−1.16	1.38	1.72
MAE	3.9	−0.80	1.44	1.67

of Table 2, that is below its thermoneutral potential, absorbing heat during charge and rejecting it during discharge.

TREC-VRFB: The figures of merit for the efficiency of a battery are the coulombic, the voltage, and the energy efficiencies ($\eta_{coulombic}$, $\eta_{voltage}$, and η_{energy}). The first represents the ratio between the amount of electrical charge supplied during charging and that recovered during discharging, and it is influenced by the crossover of vanadium species through the membrane and by the side reactions as hydrogen evolution. The voltage efficiency is given by the ratio between charging and discharging voltage and represents the electrical reversibility of the system. The product of these two efficiencies is the energy efficiency, which is the ratio between the amount of energy that can be recovered from the battery and the amount of energy that has been consumed for charging it.

Fig. 4 shows the trend for all the efficiencies for the CE and the MAE at 20 and 60 °C over several charge-discharge cycles. For CE, the average coulombic, voltage, and energy efficiency were respectively calculated to be 94%, 85%, and 79% at 20 °C and 92%, 87%, and 80% at 60 °C. In the case of MAE, the resulting efficiencies were found to be notably higher than with the CE. Indeed, they were calculated to be 98%, 88%, and 86% at 20 °C and 99%, 91%, and 90% at 60 °C. The superior performance of MAE is primarily attributed to the faster kinetics (see ESI for details). Besides, the positive shift in potential of the negative-side reaction reduces the competing hydrogen evolution improving the coulombic efficiency.

As expected, all of the efficiencies increased at higher temperatures since reaction kinetics, mass transport, and ionic conductivity all improve under these conditions (see ESI for temperature dependence of kinetics). The only discrepancy was given by the decrease of coulombic efficiency for CE. Similar effect was already observed by Zhang et al. [28] and it may be explained by the enhanced kinetics of the competing hydrogen evolution reaction on the negative side. This reaction has a large positive thermal coefficient, making it more facile at higher temperatures. Moreover, crossover of vanadium species is also enhanced at higher temperatures [29]. Interestingly this did not affect MAE as much as CE. This may be due to the fact that the negative half-cell reaction in the MAE is more positive and faster than in the CE, thus competing better with hydrogen evolution. Also the vanadium species in MAE exist as chloride complexes which may be less prone to pass through the membrane.

Fig. 5a and c show the isothermal cycles performed by the VRFB battery at 20 °C and 60 °C. For both electrolyte types, the cell voltage during the cycle shifted negatively with the increase of temperature, which is in accordance with the measured thermal coefficients. In both cases, the shift was more pronounced in the charging curve, suggesting that the kinetics of the charging reactions are more sensitive to temperature. The area between the charging curve at 60 °C and the discharging curve at 20 °C is expected to be representative of the operation of the TREC-VRFB. With CE, the energy density of the VRFB was measured to be 11.8 Wh L^{-1} at 20 °C and 11.3 Wh L^{-1} at 60 °C. In the case of MAE, the resulting energy density was 13.3 Wh L^{-1} at 20 °C and 13.2 Wh L^{-1} at 60 °C.

Fig. 5b and d illustrate the thermodynamic cycle performed by the TREC-VRFB system for both electrolytes. By using the CE, the TREC-VRFB demonstrated an increase of 9 percentage points (compared to the isothermal VRFB with CE, cycled at 20 °C) for both the overall energy efficiency and voltage efficiency (88% and 94%, respectively). As expected, the TREC clearly enhanced the performance of the battery, although the recovered energy from the TREC remained too low to fully compensate the energy loss of the conventional all-vanadium redox flow battery.

The TREC-VRFB with CE was found to reduce the energy loss of the conventional battery by 45%. The resulting increase in apparent energy density was calculated to be 1.3 Wh L^{-1}. In the case of MAE, the TREC-VRFB showed a similar reduction of energy loss of 42% compared to the conventional battery at 20 °C. Thus, the resulting apparent energy density was increased by 0.8 Wh L^{-1}. The overall energy efficiency and the voltage efficiency were determined to be 91% and 93%, respectively, corresponding to an increase of 5 percentage points of efficiency compared to the conventional battery cycle at 20 °C. In all cases, the cell voltage remained below the thermoneutral voltage, following the thermodynamic cycle described in Fig. 2.

The theoretical TREC efficiency was measured for each electrolyte using the TREC-VRFB features from Table 3, neglecting energy losses

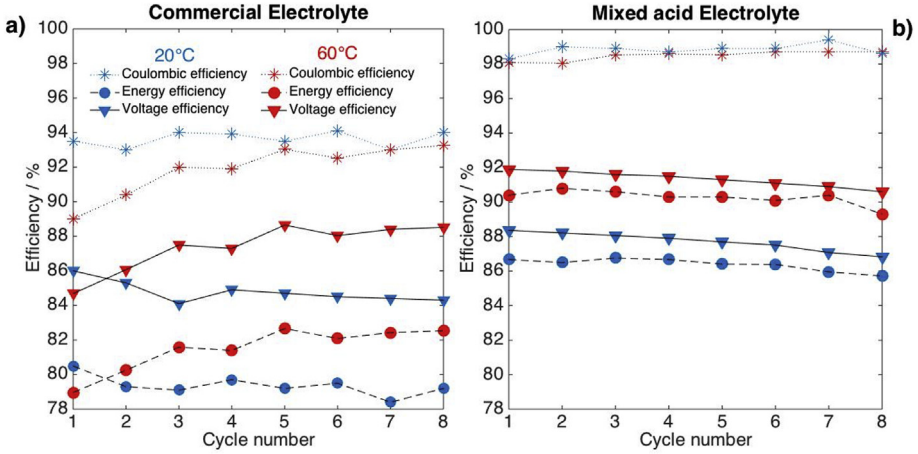

Fig. 4. Coulombic, energy, and voltage efficiency of the all-vanadium redox flow battery at 20 °C and 60 °C (a) with *commercial electrolyte* (b) and with *mixed-acid electrolyte*.

due to the battery inefficiency and the heat necessary to warm up or cool down the electrodes, membrane, current collectors, and any other part of the system apart from the electrolyte. Thus, the maximal theoretical TREC efficiency (from Eq. (10)) was calculated to be 0.92% for CE and 0.72% for MAE, whereas the Carnot efficiency (Eq. (9)) was 12%. Then, using Eq. (11), the normalized efficiency was measured, neglecting the heat transfer loss and the energy consumed by the pumps. It was 2.6% for CE and 1.7% for MAE. These values were larger than for the maximum theoretical efficiency because they consider the improvement against a standard isothermal cycle at 20 °C and not only the heat converted into electrical energy by the thermodynamic cycle.

As expected from the thermal coefficients, the TREC-VRFB recovered more energy with CE than with MAE. However, the resulting energy density in the case of MAE was higher than for CE, because the whole-cell voltage was larger. Table 4 summarizes the main performance parameters for each type of battery cycle performed.

The energy density of the TREC-VRFB was larger for both electrolytes than the isothermal energy density at 20 °C and at 60 °C. This proves that some heat was converted into electrical energy by applying the TREC. Moreover, the increase of energy density could not come solely from the increase of efficiency by employing the VRFB at higher temperatures, because although the efficiency in general increased with

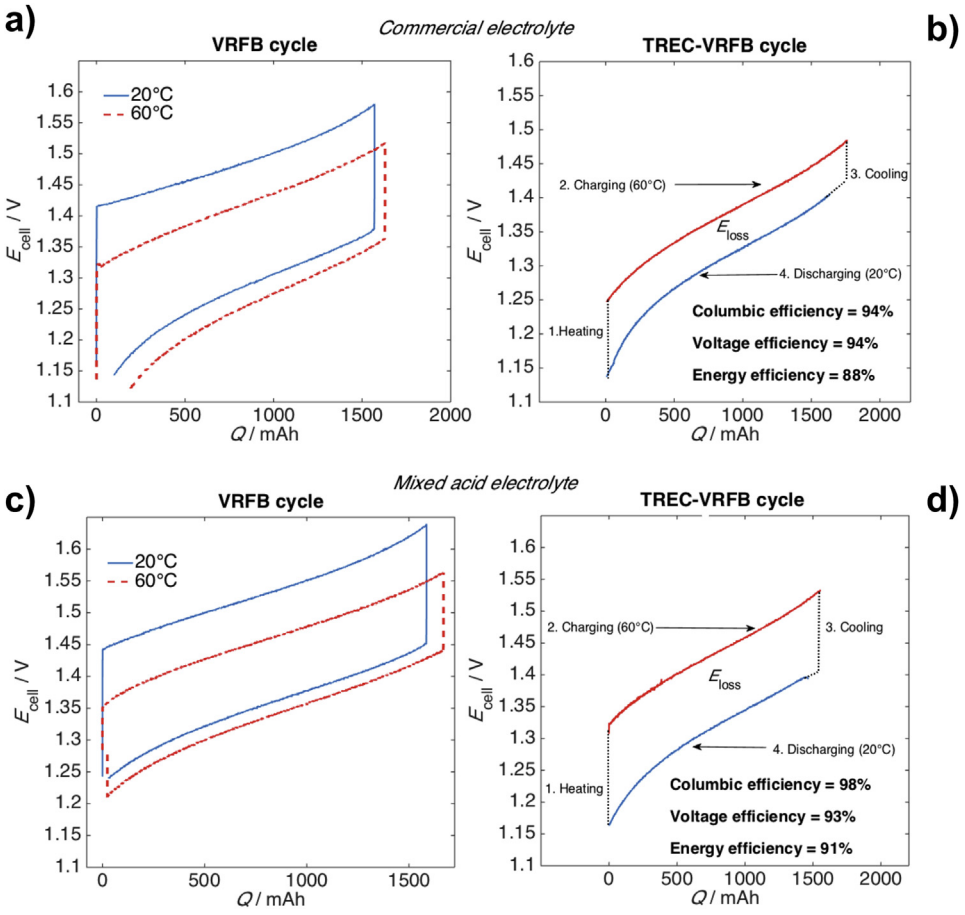

Fig. 5. Potential *versus* charge plot of the battery cycle by flowing 170 mL of electrolyte at a current density of 40mAcm^{-2} (a) VRFB cycle at 20 °C and 60 °C with *commercial electrolyte* (b) TREC-VRFB cycle between 20 °C and 60 °C with *commercial electrolyte* (c) VRFB cycle at 20 °C and 60 °C with *mixed-acid electrolyte* (d) TREC-VRFB cycle between 20 °C and 60 °C with *mixed-acid electrolyte*.

Table 4
Summary of the results for the VRFB cycle at 20 °C and 60 °C and the TREC-VRFB cycle between 20 °C and 60 °C.

	T [°C]	Energy density [Wh L^{-1}]	$\eta_{coulombic}$ [%]	$\eta_{voltage}$ [%]	η_{energy} [%]	η_{TREC} [%]	η'_{TREC} [%]
VRFB CE	20	11.8	94	85	79		
	60	11.3	92	87	80		
TREC-VRFB CE	20 to 60	13.1	94	94	88	0.92	2.6
VRFB MAE	20	13.3	98	88	86		
	60	13.2	99	91	90		
TREC-VRFB MAE	20 to 60	14.1	98	93	91	0.72	1.7

temperature, the energy density decreased for isothermal cycling at elevated temperatures.

As mentioned regarding Eq. (10), the efficiency of the TREC was limited by the ratio between heat capacity of the system and its charge density. Unlike the thermal coefficient, which is determined by the chosen chemistry, the charge density of a redox flow battery can be tuned. In fact, the concentration of vanadium in solution has a large effect on the capacity, but a small effect on the heat capacity. This is particularly advantageous in the case of MAE where the concentration of vanadium can reach 3M [10,26]. Another possible route to improve the charge density is to employ a solid-state compound in the tank which is charged and discharged by the redox species [30,31]. Therefore opening several possibilities for future implementations.

5. Conclusions

In this work, the efficiency of an all-vanadium redox flow battery (VRFB) was enhanced operating the flow battery in a Thermally Regenerative Electrochemical Cycle (TREC). Two different vanadium electrolyte systems were studied. One derived from a commercially available electrolyte containing 1 M total vanadium, 2 M H_2SO_4, 50 mM H_3PO_4, and one mixed-acid electrolyte which also contained hydrochloric acid (1 M total vanadium, 4 M HCl, 2 M H_2SO_4, 50 mM H_3PO_4). In a normal battery cycle at 20 °C, these systems showed a coulombic, voltage, and energy efficiencies of 94%, 85%, and 79% for the former and 98%, 88%, and 86% for the latter. For the TREC-based systems, the efficiency rose to 94%, 94%, and 88% and 98%, 93%, and 91%, respectively. The VRFB-TREC had a theoretical TREC-efficiency of 0.92% with the *commercial electrolyte* and 0.72% with the *mixed-acid electrolyte*, corresponding to an increase of energy density of the battery of 1.3 Wh L^{-1} and 0.8 Wh L^{-1}, respectively. The efficiency normalized against the operation at room temperature was 2.6% and 1.7%, respectively.

The need for both energy storage devices and low-grade heat recovery systems make the TREC-VRFB interesting for large-scale grid applications, particularly when the battery may be co-located with a large source of low-grade heat. Moreover, an all-vanadium redox flow battery already utilizes a fluid circulation circuit, making the thermal management easier. In the case of MAE, the possibilities to improve the system are broader than for the conventional electrolyte because of the electrolyte's higher thermal stability and vanadium solubility limit. The TREC was based on the temperature dependence of the cell voltage, which was $-1.16(8)$ mV K^{-1} for the *commercial electrolyte* and $-0.80(7)$ mV K^{-1} for the *mixed-acid electrolyte*. The systems were optimized for good thermal stability up to 60 °C with 1 M total vanadium concentration operating in the range between 10% SOC and 85% SOC.

The long charging and discharging time of RFBs (typically several hours) is well-matched for the lower heat flux available from waste-heat sources. Of course, a suitable heat sink is also necessary to reject the stored heat prior to discharging. Because of the low heat input value, the TREC-VRFB is demonstrated to be a promising approach to enhance energy density of VRFB.

Combining a VRFB-TREC with a photovoltaic farm could harvest ten percent more energy (see ESI). During the day the farm produces electricity but also heat [32]. Both of these can be used to charge the VRFB-TREC, which then can be discharged during the night when it is colder, closing the TREC cycle.

Another different implementation of a TREC-VRFB would be implementing a refrigerating cycle in which the battery is used as intermediate storage of heat. In this case, the low energy efficiency of the battery may have a lower impact on the total performance, while still conserving the direct heat to electricity paradigm.

The combination of thermally regenerative electrochemical cycles, batteries, and low-grade heat is an emerging research field and many innovations are yet to come.

Conflicts of interest

There are no conflicts to declare.

Acknowledgements

The authors acknowledge Qiwen (Carrol) Xia for her preliminary tests.

Appendix A. Supplementary data

Supplementary data related to this article can be found at http://dx.doi.org/10.1016/j.jpowsour.2018.03.074.

References

[1] M. Skyllas-Kazacos, M.H. Chakrabarti, S.A. Hajimolana, F.S. Mjalli, M. Saleem, Progress in flow battery research and development, J. Electrochem. Soc. 158 (8) (2011) R55–R79, http://dx.doi.org/10.1149/1.3599565 http://jes.ecsdl.org/content/158/8/R55.

[2] J. Zhang, M.C.W. Kintner-Meyer, X. Lu, D. Choi, J.P. Lemmon, J. Liu, Electrochemical energy storage for Green grid, Chem. Rev. 111 (5) (2011) 3577–3613, http://dx.doi.org/10.1021/cr100290v https://doi.org/10.1021/cr100290v.

[3] C.R. Dennison, H. Vrubel, V. Amstutz, P. Peljo, K.E. Toghill, H.H. Girault, Redox flow batteries, hydrogen and distributed storage, Chimia 69 (12) (2015) 753–758, http://dx.doi.org/10.2533/chimia.2015.753.

[4] P. Peljo, H. Vrubel, V. Amstutz, J. Pandard, J. Morgado, A. Santasalo-Aarnio, D. Lloyd, F. Gumy, C.R. Dennison, K.E. Toghill, H.H. Girault, All-vanadium dual circuit redox flow battery for renewable hydrogen generation and desulfurisation, Green Chem. 18 (6) (2016) 1785–1797, http://dx.doi.org/10.1039/C5GC02196K http://pubs.rsc.org/en/content/articlelanding/2016/gc/c5gc02196k.

[5] P. Alotto, M. Guarnieri, F. Moro, Redox flow batteries for the storage of renewable energy: a review, Renew. Sustain. Energy Rev. 29 (2014) 325–335, http://dx.doi.org/10.1016/j.rser.2013.08.001 http://www.sciencedirect.com/science/article/pii/S1364032113005418.

[6] H. Zhao, Q. Wu, S. Hu, H. Xu, C.N. Rasmussen, Review of energy storage system for wind power integration support, Appl. Energy 137 (2015) 545–553, http://dx.doi.org/10.1016/j.apenergy.2014.04.103 http://www.sciencedirect.com/science/article/pii/S0306261914004668.

[7] A.Z. Weber, M.M. Mench, J.P. Meyers, P.N. Ross, J.T. Gostick, Q. Liu, Redox flow batteries: a review, J. Appl. Electrochem. 41 (10) (2011) 1137, http://dx.doi.org/10.1007/s10800-011-0348-2 http://link.springer.com/article/10.1007/s10800-011-0348-2.

[8] M. Skyllas-Kazacos, L. Cao, M. Kazacos, N. Kausar, A. Mousa, Vanadium electrolyte studies for the vanadium redox BatteryA review, ChemSusChem 9 (13) (2016) 1521–1543, http://dx.doi.org/10.1002/cssc.201600102 http://onlinelibrary.wiley.com/doi/10.1002/cssc.201600102/abstract.

[9] N. Kausar, A. Mousa, M. Skyllas-Kazacos, The effect of additives on the high-temperature stability of the vanadium redox flow battery positive electrolytes, ChemElectroChem 3 (2) (2016) 276–282, http://dx.doi.org/10.1002/celc.

201500453 http://onlinelibrary.wiley.com/doi/10.1002/celc.201500453/abstract.
[10] S. Kim, E. Thomsen, G. Xia, Z. Nie, J. Bao, K. Recknagle, W. Wang, V. Viswanathan, Q. Luo, X. Wei, A. Crawford, G. Coffey, G. Maupin, V. Sprenkle, 1 kW/1 kWh advanced vanadium redox flow battery utilizing mixed acid electrolytes, J. Power Sources 237 (2013) 300–309, http://dx.doi.org/10.1016/j.jpowsour.2013.02.045 http://www.sciencedirect.com/science/article/pii/S0378775313003182.
[11] L. Li, S. Kim, W. Wang, M. Vijayakumar, Z. Nie, B. Chen, J. Zhang, G. Xia, J. Hu, G. Graff, J. Liu, Z. Yang, A stable vanadium redox-flow battery with high energy density for large-scale energy storage, Adv. Energy Mat. 1 (3) (2011) 394–400, http://dx.doi.org/10.1002/aenm.201100008 http://onlinelibrary.wiley.com/doi/10.1002/aenm.201100008/abstract.
[12] R. Hu, B.A. Cola, N. Haram, J.N. Barisci, S. Lee, S. Stoughton, G. Wallace, C. Too, M. Thomas, A. Gestos, M. E. d. Cruz, J.P. Ferraris, A.A. Zakhidov, R.H. Baughman, Harvesting waste thermal energy using a carbon-nanotube-based thermo-electrochemical cell, Nano Lett. 10 (3) (2010) 838–846, http://dx.doi.org/10.1021/nl903267n https://doi.org/10.1021/nl903267n.
[13] S.W. Lee, Y. Yang, H.-W. Lee, H. Ghasemi, D. Kraemer, G. Chen, Y. Cui, An electrochemical system for efficiently harvesting low-grade heat energy, Nat. Commun. 5 (2014) 3942, http://dx.doi.org/10.1038/ncomms4942 http://www.nature.com/ncomms/2014/140521/ncomms4942/full/ncomms4942.html.
[14] A.P. Straub, N.Y. Yip, S. Lin, J. Lee, M. Elimelech, Harvesting low-grade heat energy using thermo-osmotic vapour transport through nanoporous membranes, Nat. Energy 1 (2016) 16090, http://dx.doi.org/10.1038/nenergy.2016.90 http://www.nature.com/articles/nenergy201690.
[15] H.L. Chum, R.A. Osteryoung, Review of Thermally Regenerative Electrochemical Systems, Solar Energy Research Inst., Golden, CO (USA), 1981 State Univ. of New York, Buffalo (USA) https://www.osti.gov/scitech/biblio/6168964.
[16] Y. Yang, J. Loomis, H. Ghasemi, S.W. Lee, Y.J. Wang, Y. Cui, G. Chen, Membrane-free battery for harvesting low-grade thermal energy, Nano Lett. 14 (11) (2014) 6578–6583, http://dx.doi.org/10.1021/nl5032106 https://doi.org/10.1021/nl5032106.
[17] Y. Yang, S.W. Lee, H. Ghasemi, J. Loomis, X. Li, D. Kraemer, G. Zheng, Y. Cui, G. Chen, Charging-free electrochemical system for harvesting low-grade thermal energy, Proc. Natl. Acad. Sci. Unit. States Am. 111 (48) (2014) 17011–17016, http://dx.doi.org/10.1073/pnas.1415097111 http://www.pnas.org/content/111/48/17011.
[18] A. Hrtel, M. Janssen, D. Weingarth, V. Presser, R. v. Roij, Heat-to-current conversion of low-grade heat from a thermocapacitive cycle by supercapacitors, Energy Environ. Sci. 8 (8) (2015) 2396–2401, http://dx.doi.org/10.1039/C5EE01192B http://pubs.rsc.org/en/content/articlelanding/2015/ee/c5ee01192b.
[19] R. Long, B. Li, Z. Liu, W. Liu, Multi-objective optimization of a continuous thermally regenerative electrochemical cycle for waste heat recovery, Energy 93 (Part 1) (2015) 1022–1029, http://dx.doi.org/10.1016/j.energy.2015.09.098 http://www.sciencedirect.com/science/article/pii/S0360544215013080.
[20] X. Zhu, M. Rahimi, C.A. Gorski, B. Logan, A thermally-regenerative ammonia-based flow battery for electrical energy recovery from waste heat, ChemSusChem 9 (8) (2016) 873–879, http://dx.doi.org/10.1002/cssc.201501513.
[21] F. La Mantia, M. Pasta, H.D. Deshazer, B.E. Logan, Y. Cui, Batteries for efficient energy extraction from a water salinity difference, Nano Lett. 11 (4) (2011) 1810–1813, http://dx.doi.org/10.1021/nl200500s.
[22] J. Newman, K.E. Thomas-Alyea, Electrochemical Systems, third ed., John Wiley & Sons, 2012.
[23] M. Pasta, A. Battistel, F.L. Mantia, Batteries for lithium recovery from brines, Energy Environ. Sci. 5 (11) (2012) 9487–9491, http://dx.doi.org/10.1039/C2EE22977C http://pubs.rsc.org/en/content/articlelanding/2012/ee/c2ee22977c.
[24] M. Ye, M. Pasta, X. Xie, Y. Cui, C.S. Criddle, Performance of a mixing entropy battery alternately flushed with wastewater effluent and seawater for recovery of salinity-gradient energy, Energy Environ. Sci. 7 (7) (2014) 2295–2300, http://dx.doi.org/10.1039/C4EE01034E http://pubs.rsc.org/en/Content/ArticleLanding/2014/EE/C4EE01034E.
[25] S. Kim, M. Vijayakumar, W. Wang, J. Zhang, B. Chen, Z. Nie, F. Chen, J. Hu, L. Li, Z. Yang, Chloride supporting electrolytes for all-vanadium redox flow batteries, Phys. Chem. Chem. Phys. 13 (40) (2011) 18186–18193, http://dx.doi.org/10.1039/C1CP22638J http://pubs.rsc.org/en/content/articlelanding/2011/cp/c1cp22638j.
[26] G. Wang, J. Chen, X. Wang, J. Tian, H. Kang, X. Zhu, Y. Zhang, X. Liu, R. Wang, Study on stabilities and electrochemical behavior of V(V) electrolyte with acid additives for vanadium redox flow battery, J. Energy Chem. 23 (1) (2014) 73–81, http://dx.doi.org/10.1016/S2095-4956(14)60120-0 http://www.sciencedirect.com/science/article/pii/S2095495614601200.
[27] S.G. Bratsch, Standard electrode potentials and temperature coefficients in water at 298.15 K, J. Phys. Chem. Ref. Data 18 (1) (1989) 1–21, http://dx.doi.org/10.1063/1.555839 http://scitation.aip.org/content/aip/journal/jpcrd/18/1/10.1063/1.555839.
[28] C. Zhang, T.S. Zhao, Q. Xu, L. An, G. Zhao, Effects of operating temperature on the performance of vanadium redox flow batteries, Appl. Energy 155 (Supplement C) (2015) 349–353, http://dx.doi.org/10.1016/j.apenergy.2015.06.002 http://www.sciencedirect.com/science/article/pii/S0306261915007473.
[29] C. Sun, J. Chen, H. Zhang, X. Han, Q. Luo, Investigations on transfer of water and vanadium ions across Nafion membrane in an operating vanadium redox flow battery, J. Power Sources 195 (3) (2010) 890–897, http://dx.doi.org/10.1016/j.jpowsour.2009.08.041 http://www.sciencedirect.com/science/article/pii/S0378775309014153.
[30] Q. Huang, H. Li, M. Grtzel, Q. Wang, Reversible chemical delithiation/lithiation of LiFePO4: towards a redox flow lithium-ion battery, Phys. Chem. Chem. Phys. 15 (6) (2013) 1793–1797, http://dx.doi.org/10.1039/C2CP44466F http://pubs.rsc.org/en/content/articlelanding/2013/cp/c2cp44466f.
[31] E. Zanzola, C.R. Dennison, A. Battistel, P. Peljo, H. Vrubel, V. Amstutz, H.H. Girault, Redox solid energy boosters for flow batteries: polyaniline as a case study, Electrochim. Acta 235 (Supplement C) (2017) 664–671, http://dx.doi.org/10.1016/j.electacta.2017.03.084 http://www.sciencedirect.com/science/article/pii/S0013468617305509.
[32] T.T. Chow, A review on photovoltaic/thermal hybrid solar technology, Appl. Energy 87 (2) (2010) 365–379 https://doi.org/10.1016/j.apenergy.2009.06.037 http://www.sciencedirect.com/science/article/pii/S0306261909002761.